We are IntechOpen, the world's leading publisher of Open Access books Built by scientists, for scientists

4,800
Open access books available

122,000
International authors and editors

135M
Downloads

Our authors are among the

154
Countries delivered to

TOP 1%
most cited scientists

12.2%
Contributors from top 500 universities

CLARIVATE ANALYTICS BOOK CITATION INDEX INDEXED

WEB OF SCIENCE™

Selection of our books indexed in the Book Citation Index in Web of Science™ Core Collection (BKCI)

Interested in publishing with us?
Contact book.department@intechopen.com

Numbers displayed above are based on latest data collected.
For more information visit www.intechopen.com

24

Robust Algorithms Applied for Shunt Power Quality Conditioning Devices

João Marcos Kanieski[1,2,3], Hilton Abílio Gründling[2] and Rafael Cardoso[3]
[1]*Embrasul Electronic Industry*
[2]*Federal University of Santa Maria - UFSM*
[3]*Federal University of Technology - Paraná - UTFPR*
Brazil

1. Introduction

The most common approach to design active power filters and its controllers is to consider the plant to be controlled as the coupling filter of the active power filter. The load dynamics and the line impedances are usually neglected and considered as perturbations in the mathematical model of the plant. Thus, the controller must be able to reject these perturbations and provide an adequate dynamic behavior for the active power filter. However, depending on these perturbations the overall system can present oscillations and even instability. These effects have been reported in literature (Akagi, 1997), (Sangwongwanich & Khositkasame, 1997), (Malesani et al., 1998). The side effects of the oscillations and instability are evident in damages to the bank of capacitors, frequent firing of protections and damage to line isolation, among others (Escobar et al., 2008).

Another problem imposed by the line impedance is the voltage distortion due the circulation of non-sinusoidal current. It degrades the performance of the active power filters due its effects on the control and synchronization systems involved. The synchronization problem under non-sinusoidal voltages can be verified in (Cardoso & Gründling, 2009). The line impedance also interacts with the switch commutations that are responsible for the high frequency voltage ripple at the point of common coupling (PCC) as presented in (Casadei et al., 2000).

Due the effects that line impedance has on the shunt active filters, several authors have been working on its identification or on developing controllers that are able to cope with its side effects. The injection of a small current disturbance is used in (Palethorpe et al., 2000) and (Sumner et al., 2002) to estimate the line impedance. A similar approach, with the aid of Wavelet Tranform is used in (Sumner et al., 2006). Due to line impedance voltage distortion, (George & Agarwal, 2002) proposed a technique based on Lagrange multipliers to optimize the power factor while the harmonic limits are satisfied. A controller designed to reduce the perturbation caused by the mains voltage in the model of the active power filter is introduced in (Valdez et al., 2008). In this case, the line impedances are not identified. The approach is intended to guarantee that the controller is capable to reject the mains perturbation.

Therefore, the line impedances are a concern for the active power filters designers. As shown, some authors choose to measure (estimate or identify) the impedances. Other authors prefer

to deal with this problem by using an adequate controller that can cope with this uncertainty or perturbation. In this chapter the authors use the second approach. It is employed a Robust Model Reference Adaptive Controller and a fixed Linear Quadratic Regulator with a new mathematical model which inserts robustness to the system. The new LQR control scheme uses the measurement of the common coupling point voltages to generate all the additional information needed and no disturbance current is used in this technique.

2. Model of the plant

The schematic diagram of the power quality conditioning device, consisting of a DC source of energy and a three-phase/three-legs voltage source PWM inverter, connected in parallel to the utility, is presented in Fig 1.

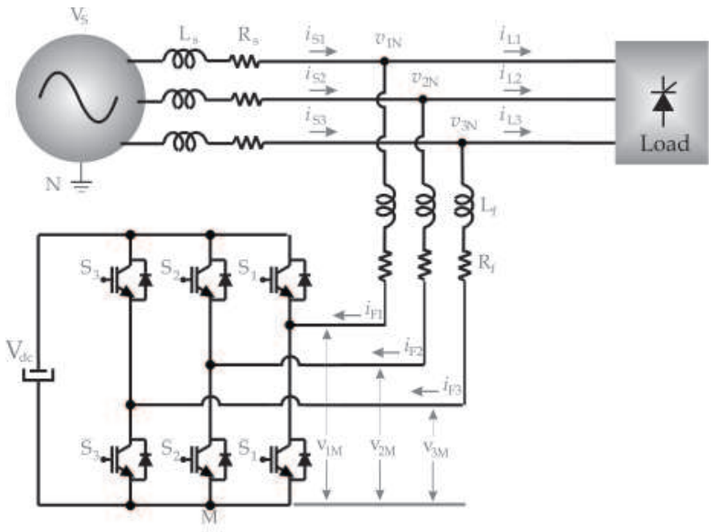

Fig. 1. Schematic diagram of the power quality conditioning device.

The Kirchoff's laws for voltage and current, applied at the PCC, allow us to write the 3 following differential equations in the "123" frame,

$$v_{1N} = L_f \frac{di_{F1}}{dt} + R_f i_{F1} + v_{1M} + v_{MN}, \tag{1}$$

$$v_{2N} = L_f \frac{di_{F2}}{dt} + R_f i_{F2} + v_{2M} + v_{MN}, \tag{2}$$

$$v_{3N} = L_f \frac{di_{F3}}{dt} + R_f i_{F3} + v_{3M} + v_{MN}. \tag{3}$$

The state space variables in the "123" frame have sinusoidal waveforms in steady state. In order to facilitate the control efforts of this system, the model may be transformed to the rotating reference frame "dq". Such frame changing is made by the Park's transformation, given by (4).

$$C_{dqO}^{123} = \frac{2}{3} \begin{bmatrix} \sin(\omega t) & \sin\left(\omega t - \frac{2\pi}{3}\right) & \sin\left(\omega t - \frac{4\pi}{3}\right) \\ \cos(\omega t) & \cos\left(\omega t - \frac{2\pi}{3}\right) & \cos\left(\omega t - \frac{4\pi}{3}\right) \\ \frac{3}{2} & \frac{3}{2} & \frac{3}{2} \end{bmatrix}. \tag{4}$$

The state space variables represented in the 'dq' frame are related to the "123" frame state space variables by equations (5)-(7).

$$\left[v_d \; v_q \; v_O \right]^T = C_{dqO}^{123} \left[v_1 \; v_2 \; v_3 \right]^T, \tag{5}$$

$$\left[i_d \; i_q \; i_O \right]^T = C_{dqO}^{123} \left[i_1 \; i_2 \; i_3 \right]^T, \tag{6}$$

$$\left[d_d \; d_q \; d_O \right]^T = C_{dqO}^{123} \left[d_1 \; d_2 \; d_3 \right]^T. \tag{7}$$

The inverse process is given in equations (8)-(10),

$$\left[v_1 \; v_2 \; v_3 \right]^T = C_{123}^{dqO} \left[v_d \; v_q \; v_O \right]^T, \tag{8}$$

$$\left[i_1 \; i_2 \; i_3 \right]^T = C_{123}^{dqO} \left[i_d \; i_q \; i_O \right]^T, \tag{9}$$

$$\left[d_1 \; d_2 \; d_3 \right]^T = C_{123}^{dqO} \left[d_d \; d_q \; d_O \right]^T, \tag{10}$$

where,

$$C_{123}^{dqO} = C_{dqO}^{123\,-1} = \frac{3}{2} C_{dqO}^{123\,T}, \tag{11}$$

and d is the switching function (Kedjar & Al-Haddad, 2009). As it is a three-phase/three-wire system, the zero component of the rotating frame is always zero, thus the minimum plant model is then given by Eq. (12)

$$\frac{d}{dt} \left[i_{dq} \right] = A \left[i_{dq} \right] + B \left[d_{dq} \right] + E \left[v_{dq} \right], \tag{12}$$

where,

$$A = - \begin{bmatrix} \frac{R_f}{L_f} & -\omega \\ \omega & \frac{R_f}{L_f} \end{bmatrix}, \qquad B = - \begin{bmatrix} \frac{v_{dc}}{L_f} & 0 \\ 0 & \frac{v_{dc}}{L_f} \end{bmatrix},$$

$$E = \begin{bmatrix} \frac{1}{L_f} & 0 \\ 0 & \frac{1}{L_f} \end{bmatrix} \quad and \quad C = \begin{bmatrix} 1 & 0 \\ 0 & 1 \end{bmatrix}.$$

Eq. (12) shows the direct system state variable dependency on the voltages at the PCC, which are presented in the 'dq' frame (v_{dq}). Fig. 2 depicts the plant according to that representation. Based on the block diagram of Fig. 2, it can be seen that the voltages at the PCC have direct influence on the plant output. It suggests that the control designer has also to be careful with those signals, which are frequently disregarded on the project stage.

2.1 Influence of the line impedance on the grid voltages

In power conditioning systems' environment, the line impedance is often an unknown parameter. Moreover, it has a strong impact on the voltages at the PCC, which has its harmonic content more dependent on the load, as the grid impedance increases. Fig. 3 shows the open loop system with a three-phase rectified load connected to the grid through a variable line impedance.

As already mentioned, by increasing the line impedance values, the harmonic content of the voltages at the PCC also increases. Higher harmonic content in the voltages leads to a more

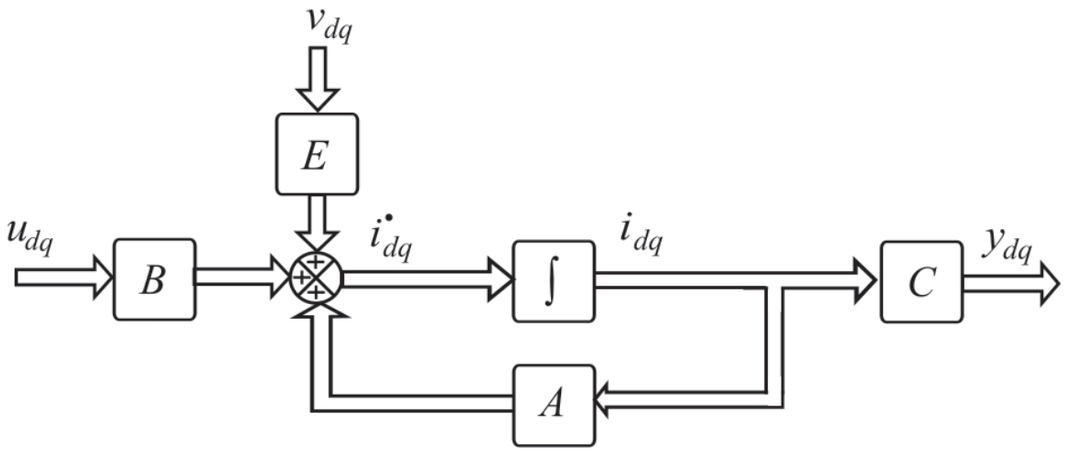

Fig. 2. Block representation of the plant.

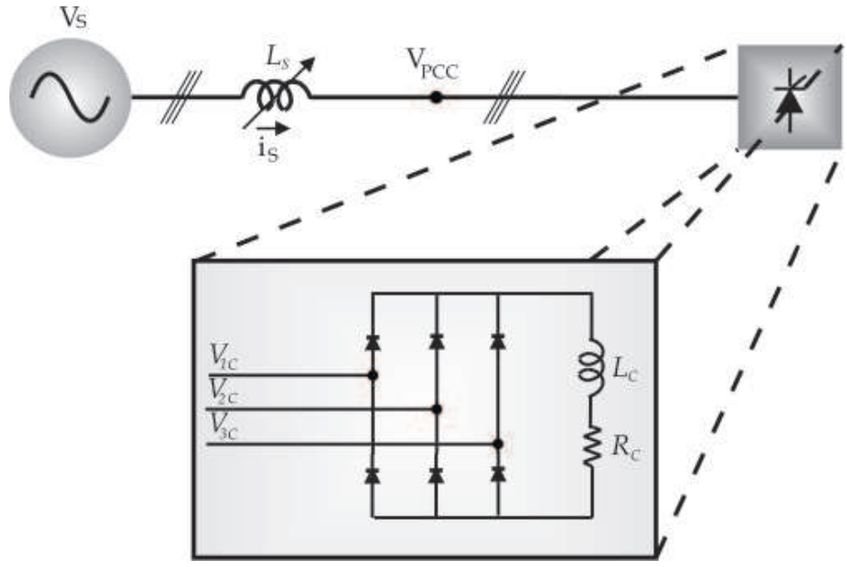

Fig. 3. Open loop system with variable line inductance

distorted waveform. It can be visualized in Fig. 4, that shows the voltage signals v_{123} at the PCC, for a line inductance of $L_S = 2mH$.

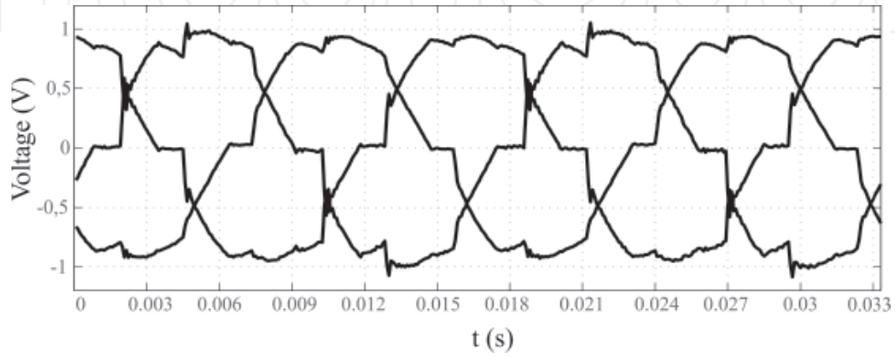

Fig. 4. Open loop voltages at the PCC with line inductance of $L_S = 2mH$.

Fig. 5 shows now an extreme case, with line inductance of $L_S = 5mH$, it is also visually perceptible the significant growth on the voltage harmonic content.

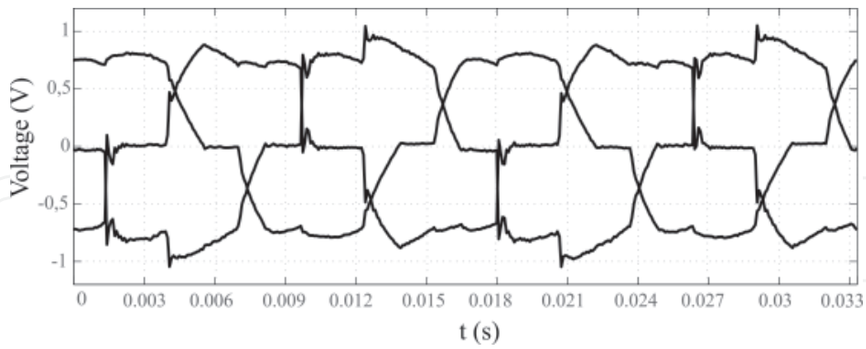

Fig. 5. Open loop voltages at the PCC with line inductance of $L_S = 5mH$.

Concluding, the voltages at the PCC have its dynamic substantially dependent on the line impedance. In other hand, the system dynamic is directly associated with the PCC voltages. Therefore, the control of this kind of system strongly depends on the behavior of the voltages at the PCC. As the output filter of the Voltage Source Inverter (VSI) has generally well-known parameters (they are defined by the designer), which are at most fixed for the linear system operation, one of the greatest control challenges of these plants is associated with the PCC voltages. The text that follows is centered on that point and proposes an adaptive and a fixed robust algorithm in order to control the chosen power conditioner device, even under load unbalance and line with variable or unknown impedance.

3. Robust Model Reference Adaptive Control (RMRAC)

The RMRAC controller has the characteristic of being designed under an incomplete knowledge of the plant. To design such controller it is necessary to obtain a representative mathematical model for the system. The RMRAC considers in its formulation a parametric model with a reduced order modeled part, as well as a multiplicative and an additive term, describing the unmodeled dynamics. The adaptive law is computed for compensating the plant parametric variation and the control strategy is robust to such unmodeled dynamics. In the present application, the uncertainties are due to the variation of the line impedance and load.

3.1 Mathematical model

From the theory presented by Ioannou & Tsakalis (1986) and by Ioannou & Sun (1995), to have an appropriated RMRAC design, the plant should be modeled in the form

$$\begin{aligned} \frac{i_F(s)}{u(s)} &= G(s) = G_0(s)[1 + \mu\Delta_m(s)] + \mu\Delta_a(s) \\ G_0(s) &= k_p \frac{Z_0(s)}{R_0(s)} \end{aligned} \tag{13}$$

where u represents the control input of the system and i_F is the output variable of interest as shown in Fig. 1.

$\Rightarrow$ Assumptions for the Plant

H1.Z_0 is a monic stable polynomial of degree $m(m \leq n-1)$,

H2.R_0 is a monic polynomial of degree n;

H3.The sign of $k_p > 0$ and the values of m, n are known.

For the unmodeled part of the plant it is assumed that:

H4.Δ_m is a stable transfer function;

H5.Δ_a is a stable and strictly proper transfer function;

H6.A lower bound $p_0 > 0$ on the stability margin $p > 0$ for which the poles of $\Delta_m(s-p)$ and $\Delta_a(s-p)$ are stable is known.

3.2 RMRAC strategy

The goal of the model reference adaptive control can be summarized as follows: Given a reference model

$$\frac{y_m}{r} = W_m(s) = k_m \frac{Z_m(s)}{R_m(s)}, \tag{14}$$

it is desired to design an adaptive controller, for $\mu > 0$ and $\mu \in [0, \mu^*)$ where the resultant closed loop system is stable and the plant output tracks, as closer as possible, the model reference output, even under the unmodeled dynamics Δ_m and Δ_a. In (14), r is a uniformly limited signal.

$\Rightarrow$ Assumptions for the model reference:

M1Z_m a monic stable polynomial of degree $m(m \leq n-1)$;

M2R_m is a monic polynomial of degree n.

The plant input is given by

$$u = \frac{\boldsymbol{\theta}^T \boldsymbol{\omega} + c_0 r}{\theta_4} \tag{15}$$

where $\boldsymbol{\theta}^T = \left[\boldsymbol{\theta}_1^T,\ \boldsymbol{\theta}_2^T,\ \theta_3\right]$, $\boldsymbol{\omega}^T = [\boldsymbol{\omega}_1,\ \boldsymbol{\omega}_2,\ y] \in \Re^{2n-1}$ and c_0 is the relation between the gain of the open loop system and the gain of the model reference. The input u and the plant output y are used to generate the signals $\boldsymbol{\omega}_1, \boldsymbol{\omega}_2 \in \Re^{n-1}$

$$\boldsymbol{\omega}_1 = \frac{\boldsymbol{\alpha}(s)}{\Lambda(s)} u \quad \text{and} \quad \boldsymbol{\omega}_2 = \frac{\boldsymbol{\alpha}(s)}{\Lambda(s)} y. \tag{16}$$

$\Rightarrow$ Assumptions for the signals ω_1 and ω_2:

R1.The polynomial Λ in (16) is a monic Hurwitz of degree $n-1$, containing stable eigenvalues.

R2.For $n \geq 2$, $\boldsymbol{\alpha} \triangleq \left[s^{n-2}, \ldots,\ s,\ 1\right]^T$ and for $n = 1$, $\boldsymbol{\alpha} \triangleq 0$.

For the adaptation of the control action parameters, the following modified gradient algorithm was considered

$$\dot{\boldsymbol{\theta}} = -\sigma \boldsymbol{P} \boldsymbol{\theta} - \frac{\boldsymbol{P} \boldsymbol{\zeta} \varepsilon}{m^2} \tag{17}$$

The σ-modification in 17 is given by

$$\sigma = \begin{cases} 0 & \text{if } \|\boldsymbol{\theta}\| < M_0 \\ \sigma_0 \left(\frac{\|\boldsymbol{\theta}\|}{M_0} - 1 \right) & \text{if } M_0 \leq \|\boldsymbol{\theta}\| < 2M_0 \\ \sigma_0 & \text{if } \|\boldsymbol{\theta}\| > 2M_0 \end{cases} \tag{18}$$

where $\sigma_0 > 0$ is a parameter of design. $\boldsymbol{P} = \boldsymbol{P}^T > 0$, $\varepsilon = y - y_m + \boldsymbol{\theta}^T \boldsymbol{\zeta} - W_m \nu = \boldsymbol{\phi}^T \boldsymbol{\zeta} + \mu\eta$ and M_0 is an upper limit $\|\boldsymbol{\theta}^*\|$, such that $\|\boldsymbol{\theta}^*\| + \delta_3 \leq M_0$ for a $\delta_3 > 0$. The normalization signal m is given by

$$\dot{m} = -\delta_0 m + \delta_1 \left(|u| + |y| + 1 \right) \tag{19}$$

with $m_0 > \delta_1 / \delta_0$, $\delta_1 \geq 1$ and $\delta_0 > 0$.
The normalization signal m is the parameter which ensures the robustness of the system. Looking to Eq. (15)-(19), it can be seen that when the control action u, the plant output y or both variables are large enough, the $\boldsymbol{\theta}$ parameters decreases and therefore the control action, which depends on the $\boldsymbol{\theta}$ parameters, also has its values reduced, limiting the control action as well as the system output in order to stabilize the system.

3.3 RMRAC applied for the power conditioning device

In the considered power conditioning system, as shows Eq. (12), there is a coupling between the "dq" variables. To facilitate the control strategy, which should consider a multiple input multiple output system (MIMO), it is possible to rewrite Eq. (12) as

$$\begin{aligned} L_f \tfrac{di_d}{dt} + R_f i_d &= L_f \omega i_q - v_{dc} d_{nd} + v_d \\ L_f \tfrac{di_q}{dt} + R_f i_q &= -L_f \omega i_d - v_{dc} d_{nq} + v_q \end{aligned} \tag{20}$$

Defining, the equivalent input as in Eq. (21) and (22),

$$u_d = L_f \omega i_q - v_{dc} d_{nd} + v_d \tag{21}$$

and

$$u_q = -L_f \omega i_d - v_{dc} d_{nq} + v_q, \tag{22}$$

the MIMO tracking problem, with coupled dynamics, is transformed in two single input single output (SISO) problems, with decoupled dynamics. Thus, currents i_d and i_q may be controlled independently through the inputs u_d e u_q, respectively. For the presented decoupled plant, the RMRAC controller equations are given by (23) and (24).

$$u_d = \frac{\boldsymbol{\theta}_{\boldsymbol{d}}^T \boldsymbol{\omega}_{\boldsymbol{d}} + c_0 r_d}{\theta_{4d}} \tag{23}$$

and

$$u_q = \frac{\boldsymbol{\theta}_{\boldsymbol{q}}^T \boldsymbol{\omega}_{\boldsymbol{q}} + c_0 r_q}{\theta_{4q}}. \tag{24}$$

The PWM actions (d_{nd} and d_{nq}), are obtained through Eq. (21) and (22) after computation of (23) and (24).

3.3.1 Design procedure

Before starting the procedure, lets examine the hypothesis ***H1***, ***H2***, ***M1***, ***M2***, ***R1*** and ***R2***. Firstly, as the nominal system, accordingly to Eq. (12), is a first order plant. The degrees n and m are then defined by $n = 1$ and $m = 0$. Therefore, the structure of the model reference and the dynamic of signals ω_1 and ω_2 can be determined. By ***M1*** and ***M2***, the model reference is also a first order transfer function $W_m(s)$, thus

$$W_m(s) = k_m \frac{\omega_m}{s - \omega_m}. \tag{25}$$

Furthermore, from ***R1*** and ***R2***: $\boldsymbol{\alpha} \triangleq 0$; and from Eq. (15), the control law reduces to

$$u_d = \frac{\theta_{3d} i_d + r_d}{\theta_{4d}} \tag{26}$$

and

$$u_q = \frac{\theta_{3q} i_q + r_q}{\theta_{4q}}. \tag{27}$$

From the information of the maximum order harmonic, which has to be compensated by the power conditioning device, it is possible to design the model reference, given in Eq. 25. Choosing, for example, the 35^{th} harmonic, as the last harmonic to be compensated, and $W_m(s)$ with unitary gain, the model reference parameters become $\omega_m = 35 \cdot 2 \cdot \pi \cdot 60 \approx 13195 \frac{rad}{s}$ and $k_m = 1$. Fig. 6 shows the frequency responses of the nominal plant of a power conditioning device, with parameters $L_f = 1mH$ and $R_f = 0.01\Omega$ and of a model reference with the parameters aforementioned.

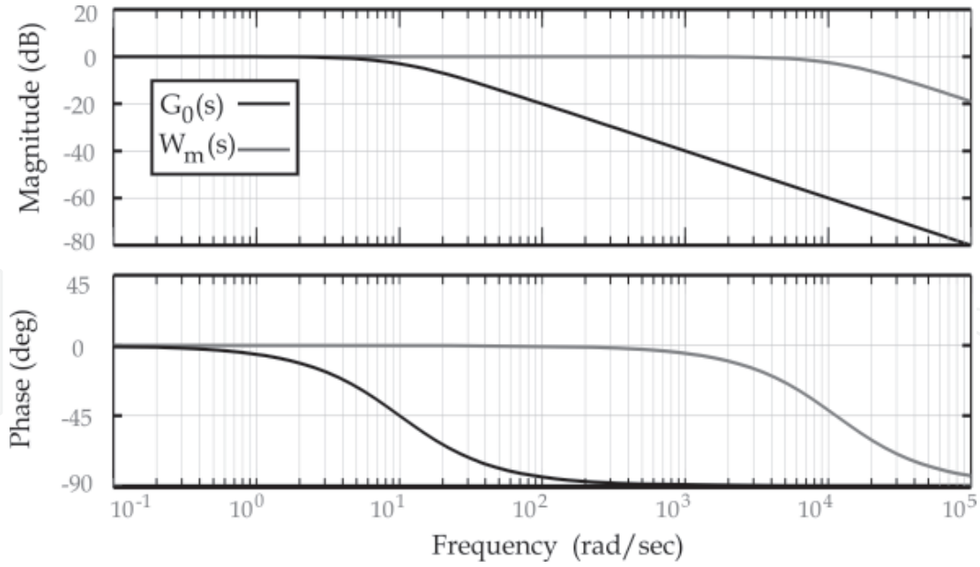

Fig. 6. Bode diagram of $G_0(s)$ and $W_m(s)$.

The vector $\boldsymbol{\theta}$ is obtained by the solution of a Model Reference Controller (MRC) for the modeled part of the plant $G_0(s)$. The design procedure of a MRC is basically to calculate the closed loop system of the nominal plant which has to be equal to the model reference transfer function.

3.3.2 RMRAC results

The RMRAC was applied to the power conditioning device, shown in Fig. 7, to control the compensation currents i_{F123}. Table 1 summarizes the parameters of the system.

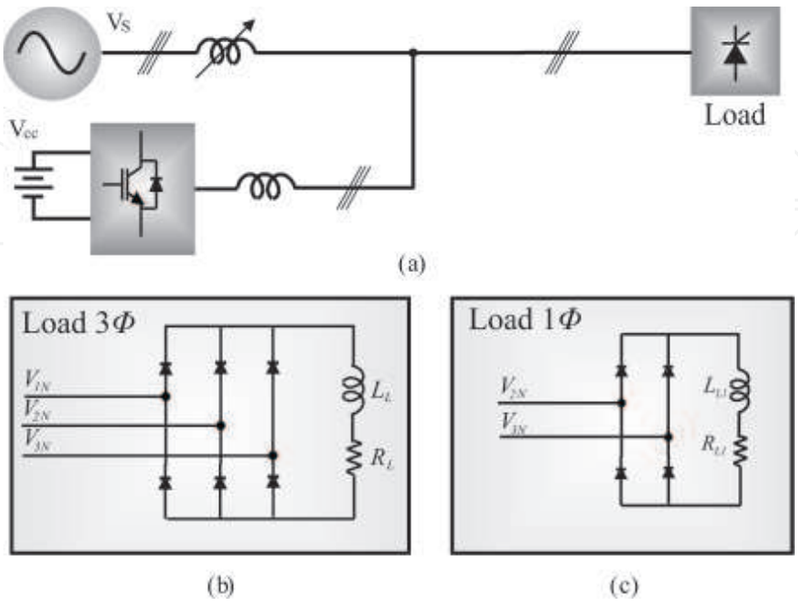

Fig. 7. Block diagram of the system.

Grid Voltage	$380V\,(RMS)$	R_f	0.01Ω
ω	$377rad/s$	L_f	$1mH$
f_s	$12kHz$	R_S	0.01Ω
V_{dc}	$550V$	L_S	$5uH$ / $2mH$ / $5mH$
$\theta_d(0)$	$[-1.02, 0.53]^T$	P	$diag\{0.99, 0.99\}$
$\theta_q(0)$	$[-1.02, 0.53]^T$	k_m	1
c_0	1	ω_m	$13195\frac{rad}{s}$
L_L	$2mH$	L_{L1}	$2mH$
R_L	25Ω	R_{L1}	25Ω

Table 1. Design Parameters

To verify the robustness of the closed loop system, which has to be stable for an appropriated range of line inductance (in the studied case: from $L_S = 5\mu H$ to $L_S = 5mH$), some simulations were carried out considering variations on the line inductance (L_S).
In the first analysis, it was considered a line impedance of $L_S = 5uH$. Fig. 8 (a) shows the load currents as well as the compensated currents, which are provided by the main source. It is also possible to see by Fig. 8 (b) the appropriate reference tracking for the RMRAC controlled system for the case of small line inductance. Fig 8 (b) shows the reference currents in black plotted with the compensation currents in gray.

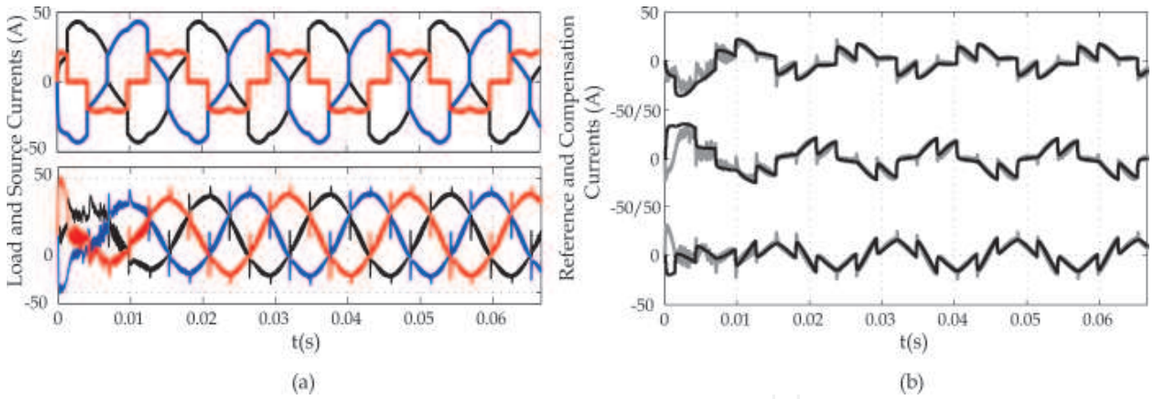

Fig. 8. System currents ($L_S = 5\mu H$): (a) Load and source currents (b) Reference and compensation currents.

In a second analysis, the line impedance was considered $L_S = 2mH$. Fig. 9 (a) shows the load currents and the compensated currents, provided by the main source. Fig. 9 (b) shows the appropriated reference tracking of the RMRAC controlled system for the case of high line inductance. Fig. 9 (b) exhibits the good tracking of the reference currents, shown in black, by the compensation currents, shown in gray.

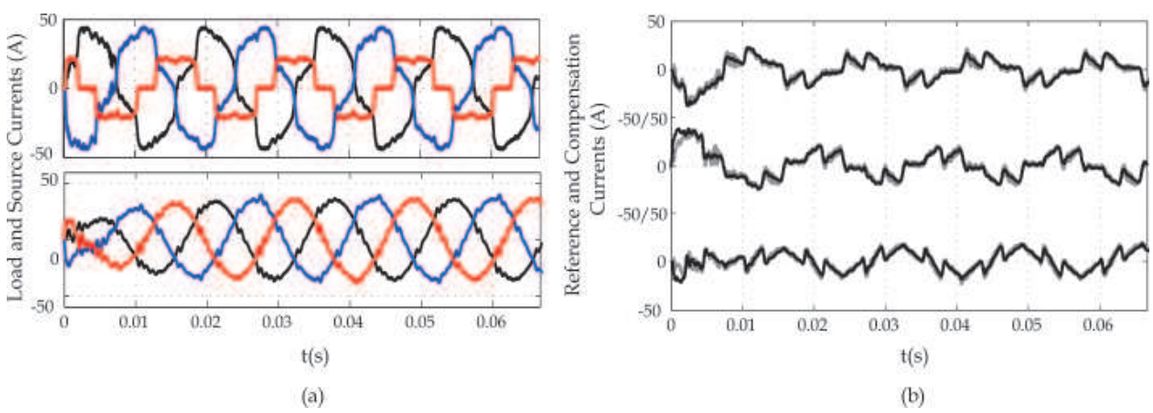

Fig. 9. System currents ($L_S = 2mH$): (a) Load and source currents (b) Reference and compensation currents.

Finally, for an extreme case of line inductance of $L_S = 5mH$, the load currents as well as the compensated currents are shown in Fig. 10 (a). Fig. 10 (b) shows the tracking performance of the RMRAC controlled system under high line impedance circumstances, which remains stable even under high inductance levels. In this figure, the reference is depicted in black and the output current is shown in gray.

Fig. 11 shows the convergence of the $\boldsymbol{\theta_d}$ and $\boldsymbol{\theta_q}$ parameters for each case of line impedance. In black, the parameters θ_{3d}, θ_{3q}, θ_{4d} and θ_{4q} for a line inductance of $L_S = 5\mu H$; in blue for a line inductance of $L_S = 2mH$; and finally, in red, for $L_S = 5mH$. In all cases the controller has an adequate convergence of its parameters.

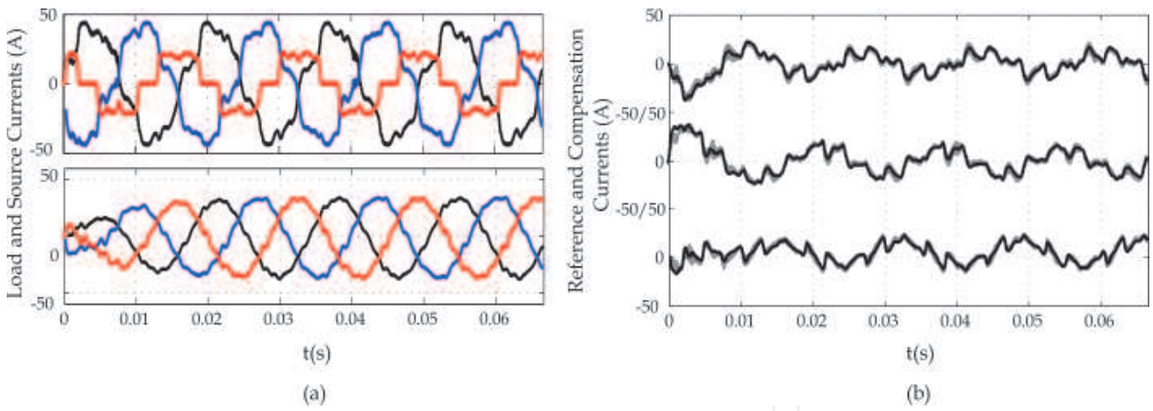

Fig. 10. System currents ($L_S = 5mH$): (a) Load and source currents (b) Reference and compensation currents.

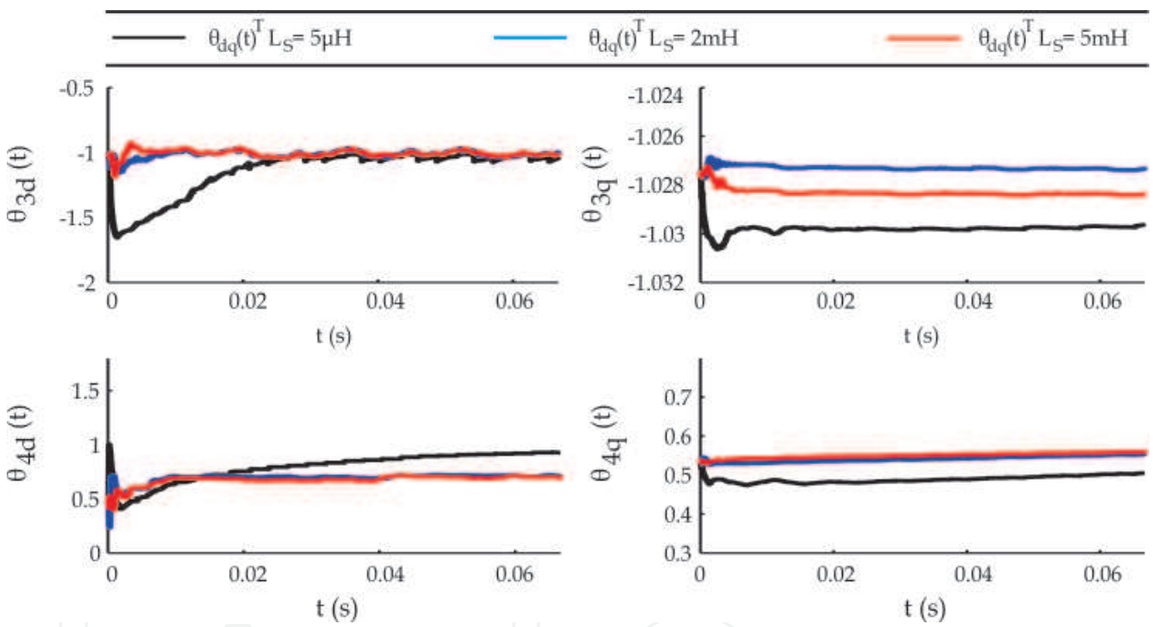

Fig. 11. Control parameters convergence.

4. A fixed robust LQR control

The Linear Quadratic Regulator (LQR) has been widely applied to several applications where optimal control is required. The LQR control strategy implementation uses state feedback where the states weighting can be chosen such the control output is properly designed to satisfy a performance criterion (Phillips & Nagle, 1995). In this control strategy, the states weighting gains are obtained through the solution of an associated algebraic Ricatti equation, which includes a performance index. The advantage of a LQR controller over other controllers found in literature is that it is designed to minimize a performance index, which can reduce the control efforts or keep the energy of some important state variable under control. Moreover, if the plant is accurately modeled, the LQR may be considered a robust controller, minimizing satisfactorily the considered states.

Consider a linear time invariant multivariable controllable system as in Eq. (28)-(29),

$$\dot{x}(t) = Ax(t) + Bu(t) \tag{28}$$

and

$$y(t) = Cx(t). \tag{29}$$

The Zero Order Hold (ZOH) discrete time model of the system with sample period T_s is

$$x_{k+1} = A_d x_k + B_d u_k \tag{30}$$

and

$$y_k = C_d x_k, \tag{31}$$

where,

$$A_d = e^{AT_s}, \quad B_d = A^{-1}(e^{AT_s} - I)B$$

and

$$C_d = C.$$

The LQR control law is given by Eq. (32)

$$u_k = -Kx_k. \tag{32}$$

and the cost function to be minimized is given by Eq. (33)

$$J = \frac{1}{2}\sum_{k=0}^{\infty} \{\ x_k^T\, Q\, x_k + u_k^T R u_k\ \}\,, \tag{33}$$

where $Q_{m\times m}$ is a positive semidefinite matrix and $R_{n\times n}$ is a positive definite matrix.
The K gains can be obtained solving the algebraic Riccati equation (Phillips & Nagle, 1995),

$$P = {A_d}^T P(A_d - B_d\ K) + Q, \tag{34}$$

$$K = (B_d^T P B_d + R)^{-1} B_d^T P A_d. \tag{35}$$

4.1 Modification on the mathematical model of the system

To achieve an adequate performance, the linear quadratic regulator needs the feedback of all significative states of the system. If there are significative disturbances in the process that can be modeled, it is plausible to include such dynamics in the state space variable set of the plant (Kanieski, Gründling & Cardoso, 2010). Considering the positive sequence of the voltages at the PCC, the equations which represent the behavior of this system can be obtained through the Laplace transform of ϕ radians delayed sines functions, given by Eq. (36):

$$v(s) = V\frac{\omega\cos(\phi) + sen(\phi)\, s}{s^2 + \omega^2}, \tag{36}$$

where V is the magnitude of the waveform considered. The state space representation of that system is given in Eq. (37),

$$\begin{bmatrix} \dot{v}(t) \\ \ddot{v}(t) \end{bmatrix} = \begin{bmatrix} 0 & 1 \\ -\omega^2 & 0 \end{bmatrix} \begin{bmatrix} v(t) \\ \dot{v}(t) \end{bmatrix}. \tag{37}$$

Thus, the three-phase sinusoidal waveforms delayed by ϕ radians can be generated by choosing the initial conditions of the voltages and its derivatives, as shown in Eq. (38),

$$\begin{array}{l} v(0) = Vsen\left(\phi\right), \\ \frac{dv(0)}{dt} = V\omega\cos\left(\phi\right). \end{array} \tag{38}$$

Therefore, the complete model that represents the voltage disturbance at the PCC of the energy storage system in the ”123” frame is presented in Eq. (39)

$$\begin{bmatrix} \dot{v}_{1N} \\ v_{2N} \\ v_{3N} \\ \dot{v}_{1N} \\ \dot{v}_{2N} \\ \dot{v}_{3N} \end{bmatrix} = M_{6x6} \begin{bmatrix} \dot{v}_{1N} \\ \dot{v}_{2N} \\ \dot{v}_{3N} \\ v_{1N} \\ v_{2N} \\ v_{3N} \end{bmatrix}, \tag{39}$$

where,

$$M_{6x6} = \begin{bmatrix} 1 & 0 & 0 & 0 & 0 & 0 \\ 0 & 1 & 0 & 0 & 0 & 0 \\ 0 & 0 & 1 & 0 & 0 & 0 \\ 0 & 0 & 0 & -\omega^2 & 0 & 0 \\ 0 & 0 & 0 & 0 & -\omega^2 & 0 \\ 0 & 0 & 0 & 0 & 0 & -\omega^2 \end{bmatrix}.$$

With equations (4), (11) and the matrix differentiation property given by Eq. (40)

$$\frac{d}{dt}\left[C_{123}^{dqO}\left[i_{dqO}\right]\right] = C_{123}^{dqO}\,\frac{d}{dt}\left[i_{dqO}\right] + \left(\frac{d}{dt}\,C_{123}^{dqO}\right)\left[i_{dqO}\right], \tag{40}$$

it is possible to derive the following ’dq’ frame model for the voltages at the PCC:

$$\begin{bmatrix} \dot{v}_d \\ \dot{v}_q \\ \ddot{v}_d \\ \ddot{v}_q \end{bmatrix} = \begin{bmatrix} 0 & 0 & 1 & 0 \\ 0 & 0 & 0 & 1 \\ -\omega^2 & 0 & 0 & \omega \\ 0 & -\omega^2 & -\omega & 0 \end{bmatrix} \begin{bmatrix} v_d \\ v_q \\ \dot{v}_d \\ \dot{v}_q \end{bmatrix}. \tag{41}$$

Thereby, the complete rotating reference frame of the considered system is given by Eq. (42)

$$\begin{bmatrix} \dot{i}_d \\ i_q \\ v_d \\ v_q \\ \dot{v}_d \\ \dot{v}_q \end{bmatrix} = \hat{A} \begin{bmatrix} i_d \\ i_q \\ v_d \\ v_q \\ \dot{v}_d \\ \dot{v}_q \end{bmatrix} + \hat{B} \begin{bmatrix} d_{nd} \\ d_{nq} \end{bmatrix}, \tag{42}$$

where,

$$\hat{A} = \begin{bmatrix} -\frac{R_f}{L_f} & \omega & \frac{1}{L_f} & 0 & 0 & 0 \\ -\omega & -\frac{R_f}{L_f} & 0 & \frac{1}{L_f} & 0 & 0 \\ 0 & 0 & 0 & 0 & 1 & 0 \\ 0 & 0 & 0 & 0 & 0 & 1 \\ 0 & 0 & -\omega^2 & 0 & 0 & \omega \\ 0 & 0 & 0 & -\omega^2 & -\omega & 0 \end{bmatrix}$$

and

$$\hat{B} = -\begin{bmatrix} \frac{v_{dc}}{L_f} & 0 \\ 0 & \frac{v_{dc}}{L_f} \\ 0 & 0 \\ 0 & 0 \\ 0 & 0 \\ 0 & 0 \end{bmatrix}.$$

Hence, the actual model may be seen as depicts Fig. 12 below, where $\hat{C}$ is such that the outputs are the 'dq' frame currents. That is,

$$\hat{C} = \begin{bmatrix} 1 & 0 \\ 0 & 1 \end{bmatrix}.$$

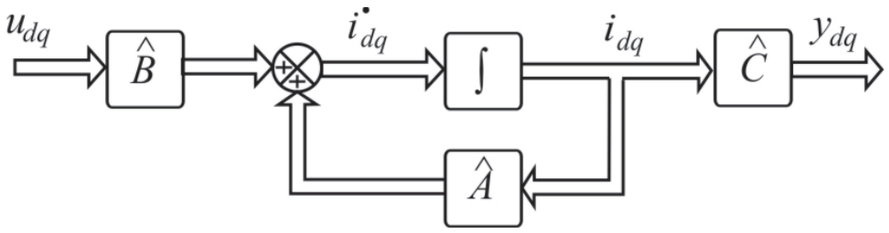

Fig. 12. Model of the system, considering the voltages at PCC as being part of the model.

4.2 LQR tuning

In the LQR tuning case, the cost function to be minimized is given by Eq. (43):

$$J_N = \frac{1}{2}\sum_{k=0}^{\infty}\left(x_{N_k}^T Q_N x_{N_k} + u_{N_k}^T R_N u_{N_k}\right). \tag{43}$$

It is perceptible, on this equation, the presence of the states related to the PCC voltages. Despite of the consideration of the voltage variables at the PCC in the plant model, for the computation of the LQR controller feedback gains, the energy related to those variables are not passible of control. Hence, those variables can not be minimized. Therefore, all the elements of the LQR matrices Q_N and R_N, related to those states, are defined as zero. The other elements are evaluated as in (Kanieski, Carati & Cardoso, 2010).

The dynamic of the states in closed loop is equal to the errors dynamics. Therefore Eq. (44) is applicable,

$$x_{N_k}^T = \left[\, e_d \; e_q \; v_d^1 \; v_q^1 \; \dot{v}_d^1 \; \dot{v}_q^1 \,\right], \tag{44}$$

which presents, as the feedback vector, the tracking errors of the states of the plant and the states related to the PCC voltages. The vector

$$u_{N_k}^T = \begin{bmatrix} d_{nd} & d_{nq} \end{bmatrix} \tag{45}$$

is the control action of the system in the "dq" frame.
With that, it is possible to obtain the following LQR matrices:

$$Q_N = \begin{bmatrix} q_{N_{11}} & 0 & 0\,0\,0\,0 \\ 0 & q_{N_{22}} & 0\,0\,0\,0 \\ 0 & 0 & 0\,0\,0\,0 \\ 0 & 0 & 0\,0\,0\,0 \\ 0 & 0 & 0\,0\,0\,0 \\ 0 & 0 & 0\,0\,0\,0 \end{bmatrix}, \qquad R_N = \begin{bmatrix} 1 & 0 \\ 0 & 1 \end{bmatrix}.$$

Fig. 13 shows the structure of the proposed LQR system. In this figure the box "KF" represents the Kalman filter estimator, which gives information about the PCC voltages, needed to compute the LQR K_N gain.

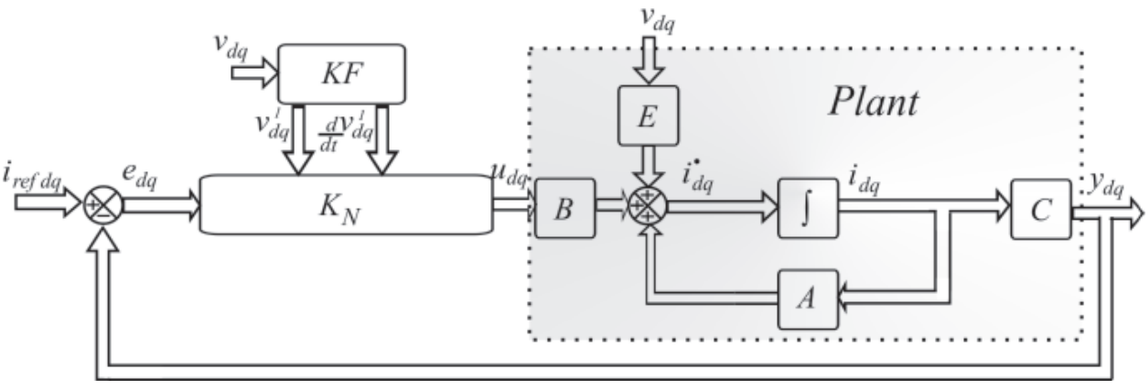

Fig. 13. Block diagram of the proposed LQR system.

5. Optimum extraction of the signal components

Using the same approach as presented in Cardoso (2008), the harmonic components of a distorted signal can be optimally extracted using a Kalman filter with an appropriate mathematical model describing the evolution of such a signal.

5.1 Modeling a signal with harmonics

The use of Kalman filter implies a model that describes the evolution of the process to be filtered. As presented by Cardoso et al. (2007) and Cardoso et al. (2008), a linear signal S_k with n harmonic components, that is,

$$S_k = \sum_{i=1}^{n} A_{i_k} \sin(i\omega_k t_k + \theta_{i_k}) \tag{46}$$

where A_{i_k}, $i\omega_k$ and θ_{i_k} are the amplitude, angular frequency and phase of each harmonic component i at the time instant t_k, has the following state-variable representation

$$\begin{bmatrix} x_1 \\ x_2 \\ \vdots \\ x_{2n-1} \\ x_{2n} \end{bmatrix}_{k+1} = \begin{bmatrix} M_1 & \cdots & 0 \\ \vdots & \ddots & \vdots \\ 0 & \cdots & M_n \end{bmatrix}_k \begin{bmatrix} x_1 \\ x_2 \\ \vdots \\ x_{2n-1} \\ x_{2n} \end{bmatrix}_k + \begin{bmatrix} \gamma_1 \\ \gamma_2 \\ \vdots \\ \gamma_{2n-1} \\ \gamma_{2n} \end{bmatrix}_k, \tag{47}$$

$$y_k = \begin{bmatrix} 1 & 0 & \cdots & 1 & 0 \end{bmatrix} \begin{bmatrix} x_1 \\ x_2 \\ \vdots \\ x_{2n-1} \\ x_{2n} \end{bmatrix}_k + \nu_k, \tag{48}$$

where

$$M_i = \begin{bmatrix} \cos(i\omega_k T_s) & \sin(i\omega_k T_s) \\ -\sin(i\omega_k T_s) & \cos(i\omega_k T_s) \end{bmatrix}, \tag{49}$$

$$x_{(2i-1)_k} = A_{i_k} \sin(i\omega_k t_k + \theta_{i_k}) \tag{50}$$

and

$$x_{2i_k} = A_{i_k} \cos(i\omega_k t_k + \theta_{i_k}). \tag{51}$$

In Eq. (47) it is considered a perturbation vector $[\gamma_1\ \gamma_2\ \cdots\ \gamma_{2n-1}\ \gamma_{2n}]_k^T$ that models amplitude or phase changes in the signal. In Eq. (48) ν_k represents the measurement noise. At the same time that the mathematical model given by equations (47)-(49) describes a signal with harmonics, it has the appropriate form necessary for the use in the Kalman filter.

The Kalman filter algorithm mentioned above will be used to generate the current references by measuring the load currents and extracting the references from it. Moreover, by measuring the voltages at the PCC, it is also possible to filter its harmonic components and, as suggests Eq. (51), the quadrature component as well. Therefore, considering that the voltage at the PCC is predominantly at the fundamental frequency, the voltage modeled in Eq. (39) is directly obtained by Eq. (50) and the derivative component is obtained by Eq. (51) multiplied by the angular frequency ω.

Fig. 14 shows the response of a Kalman filter estimator, when extracting a voltage signal and its derivative. V_{Grid} and $\dot{V}_{Grid}$, in gray, are the normalized grid voltage and its derivative. In black, $\hat{V}_{Grid}$ and $\hat{\dot{V}}_{Grid}$ are the normalized Kalman filter estimated voltage and its derivative, which, as it can be seen, presents a good performance.

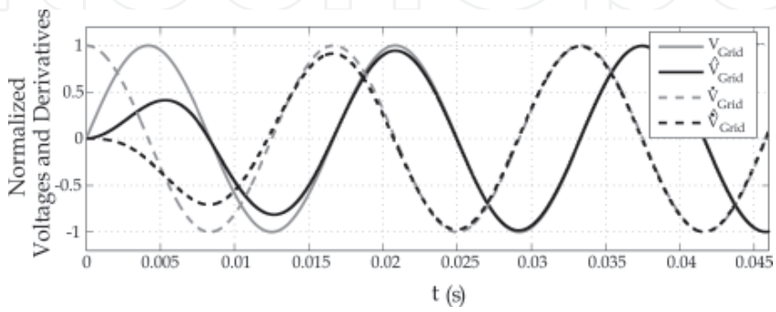

Fig. 14. Grid voltage and its derivative with their estimates provided by the Kalman filter.

5.1.1 LQR Results

The LQR control of the compensation currents i_{F123} was implemented in the same platform as presented in the RMRAC results section (section 3.3.2). Table 1 also shows the parameters used in the analysis made on this section. The Q_N and R_N matrices of the LQR controller are given by:

$$Q_N = \begin{bmatrix} 1500 & 0 & 0\,0\,0\,0 \\ 0 & 2000 & 0\,0\,0\,0 \\ 0 & 0 & 0\,0\,0\,0 \\ 0 & 0 & 0\,0\,0\,0 \\ 0 & 0 & 0\,0\,0\,0 \\ 0 & 0 & 0\,0\,0\,0 \end{bmatrix}, \qquad R_N = \begin{bmatrix} 1 & 0 \\ 0 & 1 \end{bmatrix}.$$

The same procedure that was used for the verification of the RMRAC controller was used to analyze the LQR controller performance. At first, with a small line inductance of $L_S = 5uH$, Fig. 15 (a) shows the load currents and the compensated currents, provided by the main source. The appropriated reference tracking is verified in Fig. 15 (b) for the case of small line inductance. In Fig. 15 (b), it is shown the reference currents in black, while the compensation currents are presented in gray.

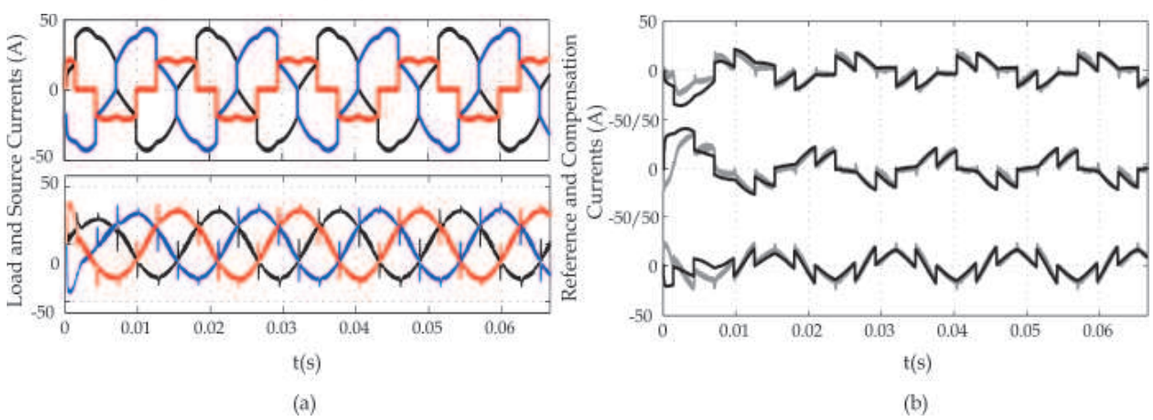

Fig. 15. System currents ($L_S = 5\mu H$): (a) Load and source currents (b) Reference and compensation currents.

In a second analysis, an inductor of $L_S = 2mH$ represents the line impedance. Fig. 16 depicts the results for this case.
Fig. 16 (a) shows the load currents and the compensated currents, provided by the main source. Fig. 16 (b) depicts good reference tracking for the system controlled by the proposed LQR scheme for the case of high line inductance.
Finally, for the case of line inductance of $L_S = 5mH$, the load currents and the compensated currents are shown in Fig. 17 (a). Fig. 17 (b) shows the tracking performance of the LQR controller, under high line impedance circumstances, which remains stable and with a good tracking performance, even under high inductance levels.

6. Conclusion

In this chapter, it was presented two robust algorithms frequently discussed in the literature, which are chosen to control the power quality conditioner due to its well known features of

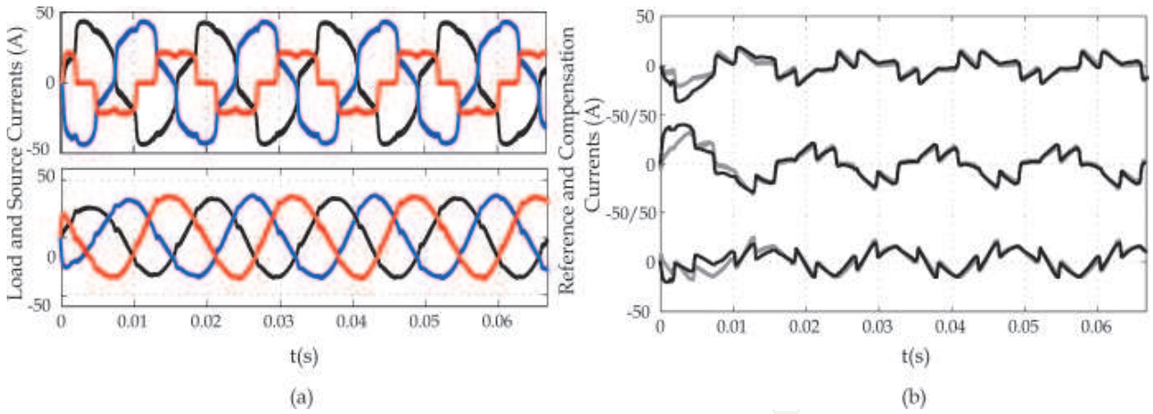

Fig. 16. System currents ($L_S = 2mH$): (a) Load and source currents (b) Reference and compensation currents.

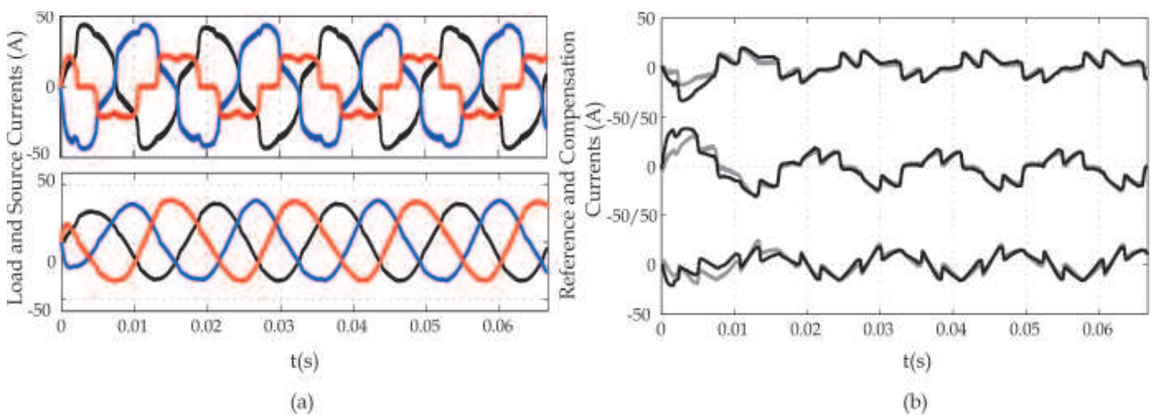

Fig. 17. System currents ($L_S = 5mH$): (a) Load and source currents (b) Reference and compensation currents.

performance and robustness: The Robust Model Reference Adaptive Controller and the fixed Linear Quadratic Regulator.

The RMRAC controller guarantees the robustness of the closed loop system by acting on the θ parameter values. The evolution of the direct axis θ parameters were presented as well as the tracking performance of the controller, for each case of line impedance ($L_S = 5\mu H$, $L_S = 2mH$ and $L_S = 5mH$), showing adequate convergence of the closed loop dynamics into the designed model reference.

For the Linear Quadratic Regulator a novel modeling approach was presented and applied to the power quality conditioning system. The scheme aimed, compared to other techniques found in literature, to have a more realistic representation of the system, by using a resonant model of the PCC voltages instead of considering it as a disturbance. The great advantage of this approach lies in having a fixed controller capable to deal with voltages disturbances, resulted from high harmonic content of load, in conditions of high line impedance. The presented mathematical model decouples the whole system, formed by the conditioner device, the main source and the load, providing an easy manner of considering just the power quality device output filter, the voltages at the PCC and its derivatives on the controller

project. The tracking performance of this fixed controller was presented, for the same three cases of line impedance tested in the RMRAC system.
The results obtained for the two cases, presented during the text, illustrated that the developed control structures exhibit good performance and robustness regarding to line inductance variation, for a huge class of loads, including those with unbalance.

7. References

Akagi, H. (1997). Control strategy and site selection of a shunt active filter for damping of harmonic propagation in power distribution systems, *IEEE Transactions on Power Delivery* 12(1): 354–363.

Cardoso, R. (2008). *Synchronization Algorithms, Power Quality Analysis And Reference Generation For Active Power Filters: A Stochastic Approach*, PhD in Electrical Engineering, Federal University of Santa Maria (UFSM).

Cardoso, R., Figueiredo, R. C., Pinheiro, H. & Gründling, H. A. (2008). Kalman filter based synchronization methods, *IET Generation, Transmission & Distribution* 2(4): 542–555.

Cardoso, R. & Gründling, H. A. (2009). Grid synchronization and voltage analysis based on the Kalman filter, *in* V. M. Moreno & A. Pigazo (eds), *Kalman Filter: Recent Advances and Applications*, I-Tech, Viena, Austria, pp. 439–460.

Cardoso, R., Kanieski, J. M., Pinheiro, H. & Gründling, H. A. (2007). Reference generation for shunt active power filters based on optimum filtering theory, *Conference Record of the 2007 IEEE Industry Applications Conference. 42nd IAS Annual Meeting*, IEEE, New Orleans, USA.

Casadei, D., Grandi, G. & Rossi, C. (2000). Effects of supply voltage non-idealities on the behavior of an active power conditioner for cogeneration systems, *Proceedings of the 31st IEEE Power Electronics Specialists Conference*, IEEE, s.l., pp. 1312–1317.

Escobar, G., Valdez, A. A. & Ortega, R. (2008). An adaptive controller for a shunt active filter considering load and line impedances, *Proceedings of the 11th IEEE International Power Electronics Congress*, IEEE, s.l., pp. 69–74.

George, S. & Agarwal, V. (2002). A novel technique for optimising the harmonics and reactive power under non-sinusoidal voltage conditions, *Proceedings of the 28th IEEE Annual Conference of the Industrial Electronics Society*, IEEE, s.l., pp. 858–863.

Ioannou, P. A. & Sun, J. (1995). *Robust Adaptive Control*, Prentice-Hall.

Ioannou, P. A. & Tsakalis, K. S. (1986). A robust direct adaptive controller, *IEEE Transactions on Automatic Control* AC-31(11): 1033–1043.

Kanieski, J. M., Carati, E. G. & Cardoso, R. (2010). An energy based lqr tuning approach applied for uninterruptible power supplies, *Proceedings of IEEE Latin American Symposium on Circuits and Systems*, IEEE, Foz do Iguaçu, Brazil.

Kanieski, J. M., Gründling, H. A. & Cardoso, R. (2010). A new lqr modeling approach for power quality conditioning devices, *Proceedings of the 36th Annual Conference of the IEEE Industrial Electronics Society*, IEEE, Phoenix, USA.

Kedjar, B. & Al-Haddad, K. (2009). Dsp-based implementation of an lqr with integral action for a three-phase three-wire shunt active power filter, *IEEE Transactions on Industrial Electronics* 56(8): 2821–2828.

Malesani, L., Mattavelli, P. & Buso, S. (1998). On the applications of active filters to generic load, *Proceedings of the International Conference on Harmonic and Quality of Power ICHQP8*, IEEE, s.l., pp. 310–319.

Palethorpe, B., Sumner, M. & Thomas, D. W. P. (2000). System impedance measurement for use with active filter control, *Proceedings of the Power Electronics and Variable Speed Drives Conference*, IEE, s.l., pp. 24–28.

Phillips, C. L. & Nagle, H. T. (1995). *Digital Control System Analysis and Design*, Prentice-Hall.

Sangwongwanich, S. & Khositkasame, S. (1997). Design of harmonic current detector and stability analysis of a hybrid parallel active filter, *Proceedings of the Power Conversion Conference*, IEEE, Nagaoka, Japan, pp. 181–186.

Sumner, M., Palethorpe, B., Zanchetta, P. & Thomas, D. W. P. (2002). Experimental evaluation of active filter control incorporating on-line impedance measurement, *Proceedings of the 10th International Harmonics and Quality of Power*, IEEE, s.l., pp. 501–506.

Sumner, M., Thomas, D. W. P. & nd P. Zanchetta, A. A. (2006). Power system impedance estimation for improved active filter control, using continuous wavelet transforms, *Proceedings of the IEEE Transmission and Distribution Conference and Exhibition*, IEEE, s.l., pp. 653–658.

Valdez, A. A., Escobar, G. & Ortega, R. (2008). A controller for the active filter considering load and line impedances, *Proceedings of the 47th IEEE Conference on Decision and Control*, IEEE, Cancun, Mexico, pp. 3749–3754.

Robust Control, Theory and Applications

Edited by Prof. Andrzej Bartoszewicz

ISBN 978-953-307-229-6
Hard cover, 678 pages
Publisher InTech
Published online 11, April, 2011
Published in print edition April, 2011

The main objective of this monograph is to present a broad range of well worked out, recent theoretical and application studies in the field of robust control system analysis and design. The contributions presented here include but are not limited to robust PID, H-infinity, sliding mode, fault tolerant, fuzzy and QFT based control systems. They advance the current progress in the field, and motivate and encourage new ideas and solutions in the robust control area.

InTech Europe
University Campus STeP Ri
Slavka Krautzeka 83/A
51000 Rijeka, Croatia
Phone: +385 (51) 770 447
Fax: +385 (51) 686 166
www.intechopen.com

InTech China
Unit 405, Office Block, Hotel Equatorial Shanghai
No.65, Yan An Road (West), Shanghai, 200040, China
中国上海市延安西路65号上海国际贵都大饭店办公楼405单元
Phone: +86-21-62489820
Fax: +86-21-62489821

IntechOpen